3.1 Determination of Interfacial Mechanical Properties of Ceramic Composites by the Compression of Micro-Pillar Test Specimens — C. Shih, Y. Katoh, K. J. Leonard, H. Bei, E. Lara-Curzio

OBJECTIVE

The objective of this work is to determine the interfacial mechanical properties of fiber matrix composites through a novel method, which involves micro compression test of micro, sized pillars containing an inclined fiber/matrix interface. These interfacial mechanical properties are important factors that affect the fracture behavior of composites. Determination of these properties is critical for modeling of composite behaviors and for designing composite with high strength and toughness.

SUMMARY

The interfacial debond shear strength and the coefficient of internal friction between the fiber and pyrocarbon interface of a SiC fiber reinforced CVI SiC matrix composite are determined using a novel method, which involves micro compression of micro sized pillars containing an inclined fiber/matrix interface. The interfacial debonds shear strength and the coefficient of internal friction was determined to be 100 MPa and 0.73, respectively. This new test method with simple geometry showed high data reproducibility; moreover, the results fit the proposed Coulomb fracture criterion well. The determined interfacial properties are compared with those determined from fiber push out tests.

PROGRESS AND STATUS

Introduction

Ceramic materials are strong, chemically inert and high temperature compatible. These unique properties make them promising for applications with extreme environments. However, the brittle nature of ceramic materials greatly limits its application. Ceramic matrix composites (CMCs) can increase the toughness and reliability of ceramic materials and have gained interest for various applications where high temperature environments are encountered, including aerospace, gas turbine, and nuclear energy [1]. The high toughness of CMCs is achieved through proper fiber/matrix (F/M) interface properties that result in arresting/deflecting of cracks formed in the matrix and sliding of the fiber during loading [2]. Therefore, designing of the F/M interface in CMCs is a critical issue for achieving good mechanical properties such as high service strength, high damage tolerance and long service life [3].

The interfacial debonds shear strength and the sliding stress of fiber pull out is the two most important parameters used for modeling of CMC properties [2, 4]. These interfacial properties can be determined by several methods including the single fiber push-out [5] or push-in tests and the tensile unloading/reloading hysteresis analysis [6]. However the uncertainty in in-situ clamping stress and complex stress state associated with Poisson effect make determination of these properties difficult.

The nano indentation technique has been widely adopted in the characterization of mechanical behavior of materials at small scales [7, 8]. Recently, this technique has extensively been used for micro- or nano-pillar compression test to study mechanical properties and deformation mechanisms of materials including metals [9-11] and monolithic ceramics [12]. In this study, a

novel test method is proposed and evaluated; where micron-sized, pillar shaped samples containing an inclined fiber/matrix interface were prepared from a SiC fiber reinforced SiC matrix composites using a focused ion beam micro-machining. The micro-pillars were then tested in a nano-indentation system equipped with a flat punch tip. This new test method employs a simple geometry and mitigates the errors associated with complex stress state.

Samples with different interface orientations were prepared and tested. The interfacial debonds shear strength and the internal friction coefficient for the interface is determined and these values are compared with those obtained by other test methods.

Experimental

Materials and micro-pillar preparation

The uni-directional single fiber-tow composite (mini-composite) used in this investigation consisted of Hi-Nicalon™ Type S SiC fibers (Nippon Carbon, Co., Ltd., Tokyo, Japan) and a b-SiC matrix. The SiC fiber has a diameter of ~11 ± 2 mm. The actual fiber diameter varies along its length. The fibers were coated with fiver layers of (50 nm pyro-carbon/1mm SiC). Both the matrix and fiber coating were synthesized by chemical vapor infiltration (CVI) by Hyper-Therm HTC, Inc (Huntington Beach, CA). The mini-composites were cut with a diamond saw and embedded in epoxy at three different angles (45, 55 and 60°) and subsequently polished using standard metallographic techniques with a series of diamond pastes to a surface finish of 100 nm. Micro-pillar test specimens were machined from the polished samples using focused iron beam (FIB) milling with a FEI (Hillsboro, OR) Qunta™ 3D 200i DualBeam™ instrument, similar to ref [13]. Initially, a large diameter annulus (~40 mm in diameter and 2 mm deep) was milled to make it easy to locate the small micro-pillars during following compression test in a nano-indentation system and to ensure that the pillars were being compressed without interference from the edge of the annulus. A beam current of 15 nA was used in the rough milling. The outer surfaces of the 3.7 mm diameter pillars containing pyrocarbon/SiC interface left standing in the middle of the annuli were then milled using a lower bean current (1 nA or less) to produce ~3.5 mm diameter cylindrical pillars. The pillar geometry is schematically shown in Fig. 1. The finished micro pillars are about 3.5 mm in diameter and at least 15mm in length. The diameter of the pillars was measured using electron beam images from the FIB system with a viewing angle along the pillar longitudinal direction. The pillars sit inside a pit that is about 40mm in diameter to accommodate the nano-indenter tip. Fig. 2 shows an electronic beam micrograph of a finished 55° interface micro-pillar before testing. The pyro-carbon interphases are readily visible and are indicated by white arrows. It can be seen that the pillar is slightly tapered because the divergence of ion beam, which was minimized as much as possible. For simplicity, this effect is not accounted for in the stress analysis.

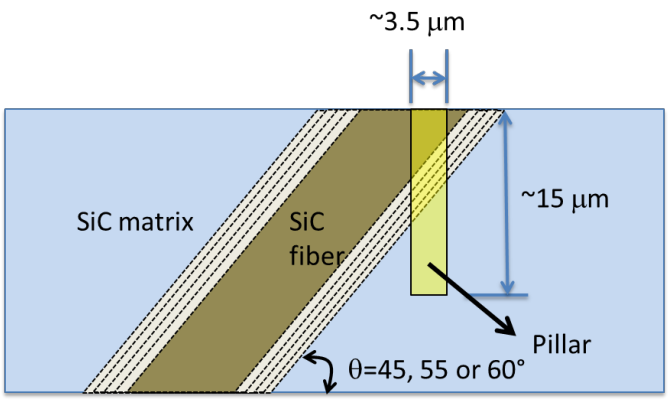

Fig. 1. A schematic plot showing the pillar geometry.

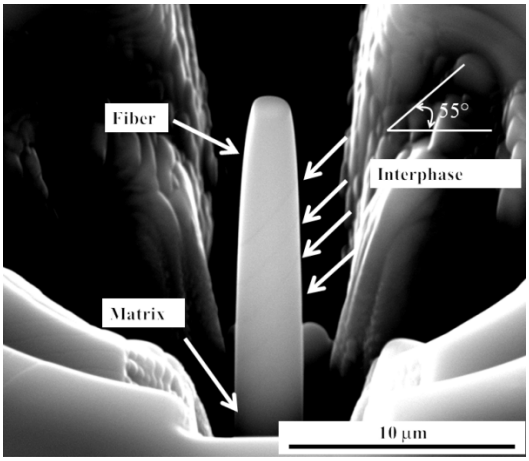

Fig. 2. Electron beam micrograph of a 55° interface micro pillar from a side angel view in the FIB.

Micro compression testing

Micro compression tests were performed with a MTS Nano XP indenter system (MTS Nano Instrument, Oak Ridge, TN) with a flat indenter tip. The flat indenter with diameter about 15 mm was custom fabricated form a conical diamond tip by using the FIB milling. The compression of the micro pillar was done under a constant load rate of 0.1 mN/sec with a data acquisition rate of 10 Hz. Details of micro-pillar testing is described in [13]. A sudden increase in displacement (strain burst) indicates that debonding and sliding along one of the interfaces has occurred. The pillars after micro compression test were examined with a field emission gun scanning electron microscope (S4800, Hitachi, Japan).

Pillar interface force balance at break

It is assumed that the pillar has a constant cross-section area, A, (ignoring the tapering effect resulting from the FIB micromachining process) and that the interface is a flat plane with an area equal to A/cosq, with q being the interface angel as shown in Fig. 1. It should be noted that the

interface has a curvature as a result of the cylindrical geometry of the fiber coatings. The load, P, from the indenter is resolved into a normal stress and a shear stress with respect to the interface as shown in Fig. 3. The Coulomb fracture criterion, which is generally used for rock failure in geology, is used as the failure criterion for this study [14]. At the pillar break load, P_{break}, the shear stress component from P should be equal to the interface debond shear stress (t_{debond}), which is related to the chemical bond strength of the interface, plus the internal friction contribution, which is estimated to be equal to the resolved normal stress times the internal friction coefficient, m. This relationship is shown in Equation 1.

$$P_{break} \cdot \frac{\sin\theta \cdot \cos\theta}{A} = \tau_{debond} + P_{break} \cdot \frac{\cos\theta \cdot \cos\theta}{A} \cdot \mu \qquad \text{(Equation 1)}$$

The Coulomb fracture criterion model predicts that in a plot of the resolved shear stress (P_{break}×sinq×cosq/A) versus resolved normal stress (P_{break}×cosq×cosq/A) at different interface angel, q, the data points should lie in a straight line with slope equal to the internal friction coefficient (m) and intersect equal to t_{debond}.

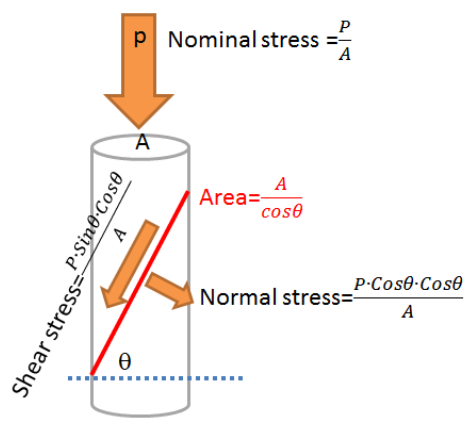

Fig. 3. Schematic showing the resovled stresses.

RESULTS AND DISCUSSIONS

Load displacement curves test

Representative load displacement curves of the micro compression tests are shown in Fig. 4. All the curves showed elastic behavior up to a breaking load, which was followed by a sudden burst of indenter displacement. The elastic behavior has been reported for CVD β-SiC micro-pillar compression tests [12]. Since all the pillars are of the same shape and materials, and since the pyrocarbon interphase layers are very thin (50 nm × five layers), the pyro carbon interphase layers with different angels are not expected to affect significantly the modulus of the pillars. Indeed, the initial slope of the load-displacement curves is the same for all the undamaged pillars (~0.077 mN/nm). The real modulus of the pillars cannot be obtained directly from the load displacement curves because the penetration of the pillar into the substrate and the load frame compliance of the machine need to be accounted for. Load displacement of a damaged pillar (sample 45°-2) is also shown in Figure 3. This pillar showed a smaller initial

slope and breaking load, indicating a damaged interface. The damage is believed to be from either the CVI process or from the high-energy ion beam during the FIB process. It is worth noting that the significant slope reduction is helpful to identify damaged pillar samples.

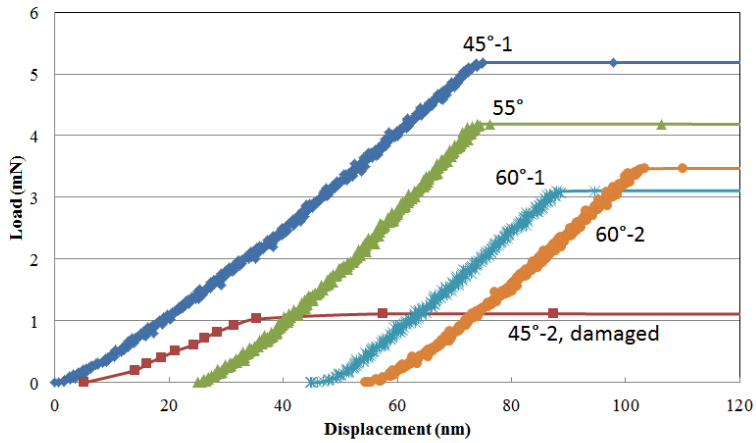

Fig. 4. Representive load displacement curves of the micro compression tests.

SEM observation following compression tests

Fig. 5 shows SEM images of two 55° micro-pillars after the compression test. The appearance of the interface angles seem different because of different specimen tilt angles in the SEM. Failure of the pillars always occurred along the innermost fiber/pyrocarbon coating interface, leaving a smooth fracture plane. It is possible that the slight taper of the micro-pillars is contributing to this trend. Energy-dispersive X-ray spectroscopy (EDS) analysis revealed the presence of a carbon rich layer on the remaining pillar fracture surface, indicating that fracture occurred between the SiC fiber and the pyrocarbon layer. This type of adhesive failure was also reported for Hi-Nicalon Type S SiC fibers reinforced CVI SiC/SiC composites under both interlaminar shear test and trans-thickness tensile test [15].

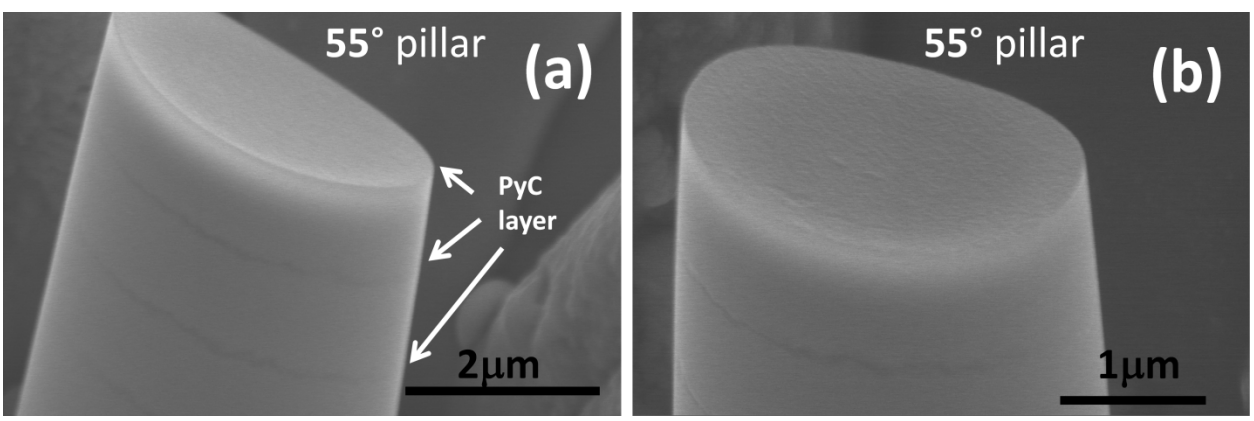

Fig. 5. SEM images of the micropillar after micro compression test.

Since a crack initiated and grew only along one interface, this test method is useful to determine the properties of that interface. It should be noted that for some fiber composites with multilayer interphase, crack propagation occurs within the PyC interphase adjacent to the fiber during fiber push in test [16], presenting a cohesive type of failure. Therefore, interfacial properties obtained from the fiber push in test and the micro pillar test correspond to different crack propagation mechanisms and should not be compared directly.

Normal and shear stress at the interface

The resolved shear stress versus the resolved normal stress plot is presented in Fig. 6 for pillars with three different interface angels. Both individual data point (triangle) and averaged values for the same inclination angle (diamond) are shown, illustrating the good degree of reproducibility. A liner fit was found to describe the data well, with a high coefficient of correlation, 0.994, which validates the applicability of the Coulomb fracture criterion described previously. The obtained interface debonds shear stress (t_{debond}) and coefficient of internal friction (m) between the pyrocarbon and SiC interface were found to be 100 MPa and 0.73, respectively, as shown in Fig. 5.

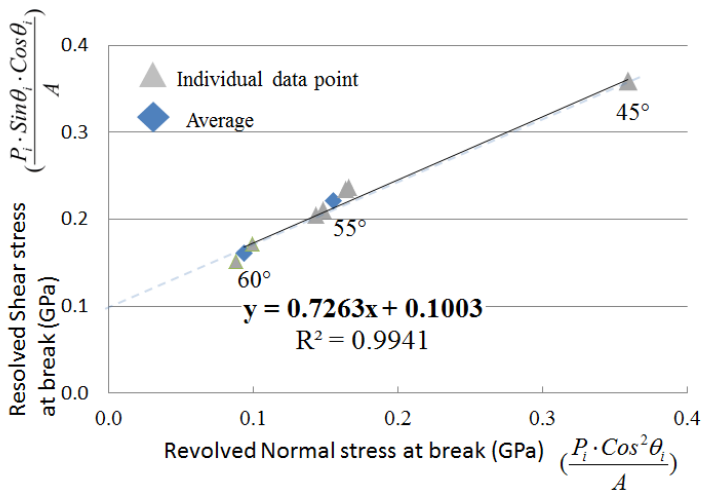

Fig. 6. Resolved shear stress versus resolved normal stress plot.

The interface debond shear stress (t_{debond}) of similar CVI SiC/SiC composite has been investigated using the fiber push in test [5] with different models [4, 17], and the reported t_{debond} is in the range of 160 to 190 MPa with large variability of 39% for the interface between Nicalon™ SiC fiber and CVI pyrocarbon. More recently, Nozawa et al. [16] reported that the interface debond shear stress of Hi-Nicalon™ Type-S SiC fiber/ CVI SiC matrix composites with a 720 nm single layer pyrocarbon interphase was found to be 280 MPa. The higher value reported for t_{debond} by the fiber push in test is partially because the push in test model doesn't account for the effect of clamping stress when debonding is initiated [4, 17, 18]. The Poisson effect during fiber push in test could also cause complex stress state and errors. The authors believe that the t_{debond} determined with the micro pillar compression method provides a value that is more representative of the chemical bonding/cohesion strength of the interface.

Pyrocarbon is generally considered to be a material of low friction coefficient. The friction coefficient between different types of SiC fibers and different thickness of pyrocarbon interphase

in SiC/SiC composites has been estimated by fitting the loading curves from fiber push out test using the Hsueh model [18]. The reported friction coefficient is in the order of 0.01 to 0.05 [5, 19], which is more than an order of magnitude smaller than the internal friction coefficient of 0.73 reported here. The authors believe that the internal friction coefficient in this study, which has been discussed extensively in geophysical research community [14], has a different physical meaning from the sliding coefficient of friction, which is well known to the materials research community. The two coefficients should not be compared directly because of their different meanings.

CONCLUSIONS

A novel test method is proposed and evaluated; where micron-sized, pillar shaped samples, containing an inclined fiber/matrix interface, were prepared and tested using the micro compression technique. The results prove that the new test method is useful for determination of interfacial debond shear strength and internal interfacial friction coefficient. The load displacement curves showed elastic behavior with similar slopes regardless if angle of inclination, and a well-defined breaking load. Out of the eight pillars prepared, only one showed pre-test damage, which was characterized by a low slope and low breaking load. Overall, this new test method shows high successful test rate and low data variability.

SEM observations showed that debonding occurred at the top fiber/pyrocarbon interface. The data points from three different interface angles fit suggest that the Coulomb fracture criterion can describe well the experimental results. The determined t_{debond} and internal friction coefficient for the SiC fiber/pyrocarbon interface are 100.3 MPa and 0.73 respectively. The determined t_{debond} appears smaller than t_{debond} from fiber push in test because the latter test uses a model that doesn't account for the effect of residual clamping stress during initial debonding. The determined internal friction coefficient of the micro pillar test was found to be an order of magnitude greater than the static friction coefficient determined by fiber push in testing and it has become clear that these two parameters have different physical meanings [14]. The new test method is simple, reproducible and complementary to other test methods. It determines interfacial properties that are important for understanding and predicting the mechanical behavior of fiber composites.

REFERENCE

[1] R. Naslain, *Compos. Sci. Technol.* **64** (2004) 155-170.
[2] A. G. Evans and D. B. Marshall, *Acta Metall.* **37** (1989) 2567-2583.
[3] R. R. Naslain, R. J. F. Pailler and J. L. Lamon, *Int. J. Appl. Ceram. Technol.* **7** (2010) 263-275.
[4] C. H. Hsueh, *Mat. Sci. Eng. A-Struct.* **123** (1990) 1-11.
[5] F. Rebillat, J. Lamon, R. Naslain, E. Lara-Curzio, M. K. Ferber and T. M. Besmann, J*. Am. Ceram. Soc.* **81** (1998) 965-978.
[6] J. M. Domergue, E. Vagaggini and A. G. Evans, *J. Am. Ceram. Soc.* **78** (1995) 2721-2731.
[7] W. C. Oliver and G. M. Pharr, *J. Mater. Res.* **19** (2004) 3-20.
[8] W. C. Oliver and G. M. Pharr, *J. Mater. Res.* **7** (1992) 1564-1583.
[9] M. D. Uchic and D. A. Dimiduk, *Mat. Sci. Eng. A-Struct.* **400** (2005) 268-278.
[10] M. D. Uchic, D. M. Dimiduk, J. N. Florando and W. D. Nix, *Sci.* **305** (2004) 986-989.
[11] C. J. Lee, J. C. Huang and T. G. Nieh, *Appl. Phys. Lett.* **91** (2007).
[12] C. Shin, H. H. Jin, W. J. Kim and J. Y. Park, *J. Am. Ceram. Soc.* **95** (2012) 2944-2950.
[13] S. Shim, H. Bei, M. K. Miller, G. M. Pharr and E. P. George, *Acta Mater.* **57** (2009) 503-510.
[14] J. Handin, *J. Geophys. Res.* **74** (1969) 5343.
[15] C. Shih, Y. Katoh, K. Ozawa, E. Lara-Curzio and L. L. Snead, *J. Am. Ceram. Soc.* **Submitted** (2012).
[16] T. Nozawa, Y. Katoh and L. L. Snead, *J. Nucl. Mater.* **367** (2007) 685-691.
[17] C. H. Hsueh, *Mat. Sci. Eng. A-Struct.* **145** (1991) 135-142.
[18] C. H. Hsueh, *J. Am. Ceram. Soc.* **76** (1993) 3041-3050.
[19] E. Lara-Curzio, M. K. Ferber and R. A. Lowden, *Ceram. Eng. Sci. Proc.* **15** (1994) 989-1000.